Monthly Notices of the ROYAL ASTRONOMICAL SOCIETY

MNRAS **470,** L107–L111 (2017)
Advance Access publication 2017 June 7

This article has been accepted for publication in Monthly Notices of the Royal Astronomical Society ©: 2017 Authors. Published by Oxford University Press on behalf of the Royal Astronomical Society. All rights reserved.

doi:10.1093/mnrasl/slx090

Detection of helicoidal motion in the optical jet of PKS 0521−365

E. F. Jiménez-Andrade,[1,2,3★] V. Chavushyan,[3] J. León-Tavares,[4] V. M. Patiño-Álvarez,[5] A. Olguín-Iglesias,[3] J. Kotilainen,[6,7] R. Falomo[8] and T. Hyvönen[9]

[1]*Argelander-Institut für Astronomie, Universität Bonn, Auf dem Hügel 71, D-53121 Bonn, Germany*
[2]*International Max Planck Research School of Astronomy and Astrophysics at the Universities of Bonn and Cologne, Germany*
[3]*Instituto Nacional de Astrofísica Óptica y Electrónica (INAOE), Apartado Postal 51 y 216, 72000 Puebla, México*
[4]*Centre for Remote Sensing and Earth Observation Processes (TAP), Flemish Institute for Technological Research (VITO), Boeretang 282, B-2400 Mol, Belgium*
[5]*Max-Planck-Institut für Radioastronomy, Auf dem Hügel 69, D-53121 Bonn, Germany*
[6]*Finnish Centre for Astronomy with ESO (FINCA), University of Turku, Väisäläntie 20, FI-21500 Kaarina, Finland*
[7]*Tuorla Observatory, Department of Physics and Astronomy, University of Turku, Väisäläntie 20, FI-21500 Kaarina, Finland*
[8]*Osservatorio Astronomico di Padova, INAF, vicolo dell'Osservatorio 5, I-35122 Padova, Italy*
[9]*Faculty of Natural Sciences, Tampere University of Technology, PO Box 589 FI-33101 Tampere, Finland*

Accepted 2017 June 5. Received 2017 May 18; in original form 2017 April 14

ABSTRACT

The jet activity of active galactic nuclei (AGNs), and its interaction with the interstellar medium, may play a pivotal role in the processes that regulate the growth and star formation of its host galaxy. Observational evidence that pinpoints the conditions of such interaction is paramount to unveil the physical processes involved. We report on the discovery of extended emission-line regions exhibiting an S-shaped morphology along the optical jet of the radio-loud AGN PKS 0521−365 ($z = 0.055$), by using long-slit spectroscopic observations obtained with FOcal Reducer/low dispersion Spectrograph 2 on the Very Large Telescope. The velocity pattern derived from the [O II] λ3727 Å, H β λ4861 Å and [O III] $\lambda\lambda$4959, 5007 Å emission lines is well fitted by a sinusoidal function of the form: $v(r) = \alpha r^{1/2} \sin(\beta r^{1/2} + \gamma)$, suggesting helicoidal motions along the jet up to distances of 20 kpc. We estimate a lower limit for the mass of the outflowing ionized gas along the jet of $\sim 10^4\,M_\odot$. Helical magnetic fields and jet precession have been proposed to explain helicoidal paths along the jet at pc scales; nevertheless, it is not clear yet whether these hypotheses may hold at kpc scales.

Key words: ISM: jets and outflows – galaxies: active – galaxies: individual: (PKS 0521−365).

1 INTRODUCTION

The energy released by active galactic nucleus (AGN) is thought to significantly impact the evolution of its host galaxy (e.g. Fabian 2012; Kormendy & Ho 2013; King & Pounds 2015). Observational evidence of winds driving gas out of the nuclear regions (e.g. Holt 2008; Harrison et al. 2012; Combes et al. 2013; Morganti et al. 2013a,b; Dasyra et al. 2015; Morganti et al. 2015; Collet et al. 2016; Querejeta et al. 2016) suggests that outflows might be the main mechanism that could efficiently transfer energy from scales close to the black hole (pc) to host galaxy scales (kpc). These outflows – which arise as a by-product of accretion on to a black hole – are usually associated with either an accretion disc or radio jets (e.g. Croton et al. 2006; Krongold et al. 2007); nevertheless, the physical processes that regulate the interplay between the radio jet activity and the multiphase gas remain unclear. On this regard, spatially resolving the interaction between an AGN and its host galaxy will provide key constraints on the physics and ubiquity of AGN feedback. For instance, long-slit spectroscopic studies have proved to be well suited to resolve jet–cloud interactions in nearby radio galaxies, suggesting strong interactions between the radio-emitting plasma and the ISM (e.g. Clark et al. 1997; Armus et al. 1998; Clark et al. 1998; Villar-Martín et al. 1999; Emonts et al. 2005; Inskip et al. 2008; Rosario et al. 2010b). On the other hand, Integral Field Spectroscopy is particularly useful to disentangle the kinematic components and ionization state of complex extended emission-line regions, which are not only limited to the radio jet-axis (e.g. Solórzano-Iñarrea & Tadhunter 2003; Inskip et al. 2008; Santoro et al. 2015).

PKS 0521−365 is one of the most studied radio-loud AGN in the southern sky. Yet, there is no robust observational evidence on the effect of the AGN activity on its host galaxy (e.g. Hyvönen et al. 2007). Therefore, it becomes one of the most accessible targets

★ E-mail: ericja@astro.uni-bonn.de

© 2017 The Authors
Published by Oxford University Press on behalf of the Royal Astronomical Society

Downloaded from https://academic.oup.com/mnrasl/article-abstract/470/1/L107/3862529
by Turun Yliopiston Kirjasto user
on 09 January 2018

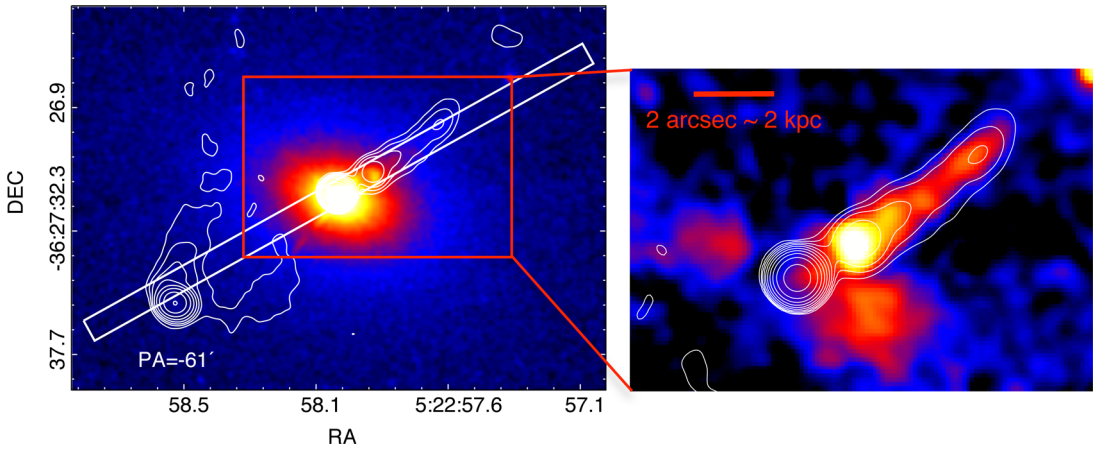

Figure 1. Left-hand panel: Optical *HST* image (WFPC2/F702W) of PKS 0521−365, which features the host galaxy emission and the prominent jet. The contours represent the VLA radio map at 15 GHz (contour levels: −1, 1, 2, 4, 8, 16, 32, 64, 128, 256 and 512 mJy beam^{-1}; Falomo et al. 2009). Solid white rectangle shows the position of the slit (PA = −61º.0). Right-hand panel: Residual image obtained after modelling and subtracting the host galaxy and nucleus contribution with GALFIT. The diffuse emission along the major axis of the host galaxy might be closely related with the structure perpendicular to the radio jet detected with ALMA (Leon et al. 2016). The contour levels correspond to the VLA radio map at 15 GHz described above.

($z = 0.055\ 48$) for spatially resolving the trace that powerful jets leave on its host galaxy. Classified as a Flat Spectrum Radio Quasar (Scarpa, Falomo & Pian 1995), it shows a large-scale optical/near-IR/sub-mm jet well aligned with the kpc radio jet (Scarpa et al. 1999; Falomo et al. 2009; Leon et al. 2016; see Fig. 1). Recently, a diffuse and extended structure perpendicular to the radio jet was detected in bands 3 and 6 with ALMA, which may be related with the relic of a previous jet or thermal (dust) emission associated with a central star-forming region (Leon et al. 2016). In this Letter, we report the discovery of extended emission-line regions exhibiting an S-shaped morphology that suggests helicoidal motions along the jet of PKS 0521−365 at kpc scales, providing new evidence on the way that AGN jets interact with the ISM. We report in Section 2 the details of the observations, followed by the results and analysis in Section 3. A discussion is given in Section 4. A cosmology with $H_0 = 70$ km s^{-1} Mpc^{-1}, $\Omega_m = 0.30$ and $\Omega_\Lambda = 0.70$ is assumed, corresponding to a luminosity distance for PKS 0521−365 of 247.6 Mpc and a scale of 1.078 kpc arcsec^{-1}.

2 OBSERVATIONS

We secured long-slit spectra along the direction of the optical jet of PKS 0521−365 (PA = −61º.0, see Fig. 1) with the Very Large Telescope (VLT), using the FOcal Reducer/low dispersion Spectrograph 2 (FORS2; Appenzeller et al. 1998) and the GRIS 600B+22 (wavelength range 3300–6210 Å, dispersion 50 Å/mm). Three consecutive spectra of integration time 850 s each were obtained during 2008 December 12 under good atmospheric conditions (seeing∼0.7; air mass∼1.1). The data reduction was performed using the standard procedures with IRAF. In the first stage, bias subtraction, flat fielding and removal of bad pixels were applied. Then, wavelength calibration, background subtraction were performed before combining the three spectra into a single spectrum. Flux calibration was performed after extracting 1D spectra along the spatial axis by using the standard star LT2415B. This result in a long-slit spectrum that encompass emission from the central engine and the optical jet with adequate spectral resolution (FWHM$_{\rm sky\text{-}lines} = 4.5$ Å) and high signal-to-noise ratio (S/N) (∼100).

To pinpoint the spatial region covered by our long-slit spectroscopic data, we also use the Hubble Space Telescope *(HST)* image of PKS 0521−365 using WFPC2 in the *R*(*F702W*) filter (Scarpa et al. 1999). The optical image was modelled using the galaxy fitting algorithm GALFIT. We use the point spread function (PSF) model, obtained with the *HST* PSF modelling tool Tiny Tim, to represent the nuclear region of the galaxy. Similarly, we used a Sérsic profile convolved with the PSF to represent the host galaxy. According to our analysis, the host galaxy of PKS 0521−365 is (as expected) a giant elliptical with a Sérsic index $n = 3.96 \pm 0.41$, an effective radius $R_e = (4.74 \pm 0.55)$ kpc, an ellipticity $E = 0.23 \pm 0.10$ and a magnitude $m = 18.13 \pm 0.52$ ($M = -18.88 \pm 0.52$), well in accordance with previous analysis on PKS 0521−365 (Urry et al. 2000) and typical values of blazars hosts (Olguín-Iglesias et al. 2016). In the right-hand panel of Fig. 1, we show the optical *HST* image when we subtract the modelled nucleus and host galaxy, revealing an optical jet that displays knotty morphologies and reassembles the structure of the radio jet.

3 RESULTS

Long-slit spectroscopy has revealed a large number of extended emission-line regions aligned with the radio jet axis of radio-loud AGN. The spatial extent, ionization state and velocity fields of these regions have been examined in some detail (e.g. Best et al. 1997; Scarpa et al. 1999; Villar-Martín et al. 1999; Emonts et al. 2005; Rosario et al. 2010a,b; Liuzzo et al. 2011). In this work, we report on the finding of extended emission-line regions along the optical jet of PKS 0521−365. In the 2D spectrum (see Figs 1 and 2), the warped and knotty emission lines [O II] λ3727 Å, H β λ4861 Å and [O III] λλ4959, 5007 Å spread along the spatial axis towards the direction of the optical jet, which suggests ongoing jet–cloud interactions. In fact, this emission corresponds to the emitting knots travelling along the jet revealed by the *HST* imaging (see Fig. 1). We do not detect extended emission in the direction of the counter-jet in our long-slit spectroscopic nor optical imaging data (see Figs 1 and 3); which might be due to the fact that relativistic beaming enhance the approaching jet flux and dim the receding one (Leon et al. 2016).

The optical 1D spectra from the optical jet emission and the central engine were obtained by co-adding emission along the spatial axis in the 2D spectrum (see Fig. 3). In the first case, we

Downloaded from https://academic.oup.com/mnrasl/article-abstract/470/1/L107/3862529
by Turun Yliopiston Kirjasto user
on 09 January 2018

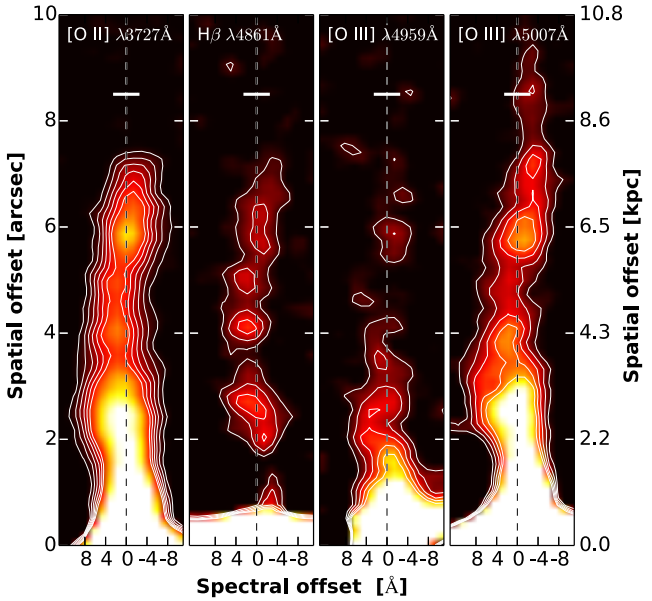

Figure 2. 2D images showing extended emission lines revealed by long-slit spectra obtained with the slit oriented along the optical jet (PA = −61.°0) – continuum emission has been subtracted. The extended emission lines [O II] λ3727 Å, H β λ4861 Å and [O III] λλ4959, 5007 Å, feature an S-shaped morphology (contour levels: 3, 6, 9, 12, 15 and 18σ). Our spectral resolution, given by the FHWM from the sky-lines of 4.5 Å, is shown in all the panels as a white horizontal line.

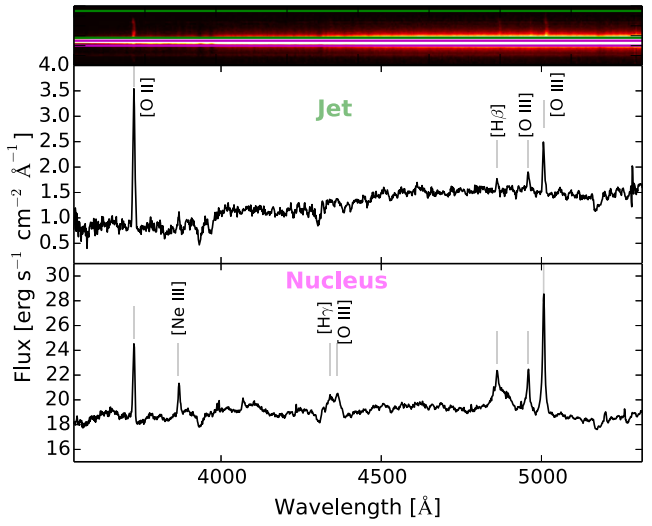

Figure 3. Upper panel: 2D spectrum of PKS 0521−365, green and magenta lines show the regions where the emission from the optical jet and the central engine were integrated. Middle panel: Spectrum from the optical jet that exhibits narrow emission lines. Lower panel: Spectrum from the inner kpc in PKS 0521−365, which shows strong emission lines from the central engine and shallow stellar absorption lines.

integrate emission spreading up to ∼10 arcsec from the nucleus and neglect that from the inner ∼1.5 arcsec, which is contaminated by broad-line emission. In physical units, this corresponds to an area of ∼8.5 × 1 kpc^2, without correcting for the jet orientation. Similarly, to get the spectrum from the central engine, we integrate emission from the inner kpc. As expected, the spectrum of the optical jet emission exhibits strong [O II] λ3727 Å and [O III] λ5007 Å narrow emission lines as well as stellar absorption features. On the other hand, the spectrum from the nucleus is dominated by the central engine with strong and broad H β λ4861 Å line emission along with narrow emission lines.

The spectral coverage of the spectra (3500–6000 Å) does not allow us to detect the [O I] λ6300 Å, H α λ6563 Å and [S II] λλ6717, 6731 Å emission lines, which are essentials to probe the physical conditions (density, temperature) and disentangle the ionization mechanism of the emitting gas by using nebular emission-line diagnostic diagrams [e.g. Baldwin, Phillips & Terlevich (BPT) diagrams]. Thus, probing the ionization state of the gas is beyond the scope of this work. Nevertheless, we profit from the intermediate spectral resolution and high S/N of our spectra to examine the radial velocity patterns of the diffuse and warped emission lines spreading along the optical jet of PKS 0521−365 (see Figs 2 and 3).

3.1 Velocity profile

To explore the kinematics of the gas clouds along the optical jet, we extract their spatial profile from the 2D spectrum. We first remove the 'contamination' by adjacent continuum emission in the 2D spectrum (which spread over a few arcsec along the spatial axis) with the task *continuum* in IRAF. We integrate the emission (detected above 3σ in the 2D spectrum) along the spatial axis in bins of 5 pixels – our spatial resolution is ∼4.5 pixels, where 1 pixel = 0.126 arcsec. A single Gaussian function is fitted to each line in order to obtain the amplitude, σ and central wavelength of the line profile; from the latter parameter, we estimate the velocity offset with respect to the systemic velocity of the host galaxy. Given that stellar features in the spectrum from the nucleus are shallow, we use narrow emission lines ([O II] λ3727 Å, [O III] λλ4959, 5007 Å) associated with the central engine to derive the systemic velocity. We do not use any constraint on the separation nor line ratio of the [O III] doublet in order to obtain independent measurements. It should be noted that the spectral resolution, given by the full width at half-maximum (FWHM) from the sky-lines (FWHM$_{\rm sky\text{-}lines}$ = 4.5 Å), suffices to resolve the emission spreading within a spectral range of ∼15 Å (in the case of [O II] λ3727 Å and [O III] λ5007 Å).

The velocity profile along the optical jet derived from the four lines is shown in Fig. 4. Although the velocity swings are evident in the 2D spectrum, we perform a chi-square goodness of fit test to explore whether our data points can be described by a constant function, $v(r) = v_{\rm c}$, where $v_{\rm c}$ is the mean velocity in km s^{-1} along the spatial axis. We derive $\chi^2 = 28$ – with 44 degrees of freedom – which yield a *p-value* of 0.035. Consequently, since the *p-value* is smaller than the significance level (0.05) we can reject the null hypothesis, meaning that the data are not consistent with a constant function. On the other hand, it should be noted that the velocity profiles remarkably resemble an S-shape suggesting a sinusoidal behaviour. Thus, for fitting the data better than a linear model, we propose a sinusoidal function (defined by three coefficients) to fit the velocity profile:

$$v(r) = \alpha r^{1/2} \sin(\beta r^{1/2} + \gamma), \quad (1)$$

where $v(r)$ is the velocity in km s^{-1}, r is the distance in kpc, and α, β and γ are constants to be determined. We use a non-linear least-squares (Levenberg-Marquardt) algorithm to find the best-fitting values for these constants: $\alpha = (64 \pm 4)$ km s^{-1} kpc$^{-1/2}$, $\beta = (-2.8 \pm 0.12)$ kpc$^{-1/2}$ and $\gamma = -11.8 \pm 0.3$. This function describes a sinusoidal movement of ionized matter along the jet; where both, amplitude and period, increase with the distance. The farthest detected emission lies at 10 kpc – without correcting by the jet orientation – and the projected velocity reaches a maximum of

Downloaded from https://academic.oup.com/mnrasl/article-abstract/470/1/L107/3862529
by Turun Yliopiston Kirjasto user
on 09 January 2018

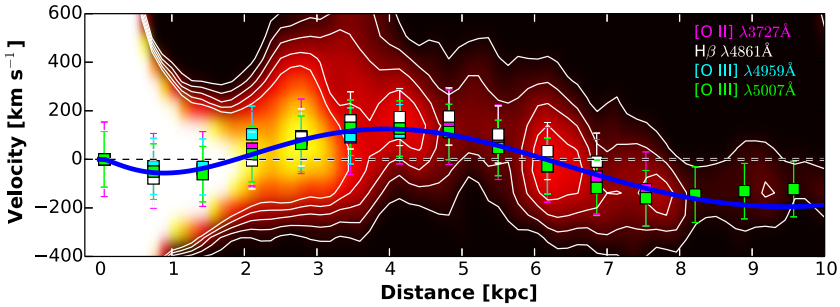

Figure 4. Velocity profile along the optical jet (PA = −61.°0) of PKS 0521−365 derived from the [O II] λ3727 Å, H β λ4861 Å and [O III] λλ4959, 5007 Å emission lines. The background image shows smoothed emission of the [O III] λ5007 Å emission line in the 2D spectrum, while the squares show the derived profiles after binning the emission along the spatial axis. The solid blue line represents the sinusoidal model to fit the data. The length of the error bars is given by the spectral resolution, i.e. $\sigma_s = \mathrm{FWHM_{sky\text{-}lines}}/(2\sqrt{2\ln(2)}) \sim 1.8$ Å. The wavelength axis has been labelled in velocity units with respect to the systemic velocity of the galaxy; while the spatial axis has been labelled in physical distance units (kpc) according to the given plate scale (0.126 arcsec pixel^{-1}) and the assumed cosmological parameters.

200 km s^{-1}. In fact, under the conservative assumption of having a viewing angle of 30° (Pian et al. 1996; Giroletti, Giovannini & other 2004) the optical emission along the jet would extend up to 20 kpc.

In order to discern if the observed velocity shifts in the emission lines are consistent with the proposed model, we apply a Kolmogorov–Smirnov (K-S) test (Press et al. 1986). We simulated a sample of distance values by Monte Carlo simulations, then velocity shift values were obtained from the sinusoidal function, for each simulated value. By comparing the observations to the generated sample drawn from a distribution based on the sinusoidal model, we obtained a K-S statistic of 0.15 and a significance level of the K-S statistic of 0.61. Such high significance level points towards the null hypothesis being correct. From the K-S analysis, we conclude that both samples, observed and simulated, are drawn from the same parent distribution; which strengthens the argument of the sinusoidal motion along the jet.

3.2 Mass outflow along the jet

If the gas in a line-emitting region is primarily photoionized, the mass of the gas can be estimated from the H β luminosity as follows (Osterbrock 1989):

$$M_{\mathrm{gas}} = m_{\mathrm{p}} \frac{L(\mathrm{H}\beta)}{n_{\mathrm{e}} \alpha^{\mathrm{eff}}_{\mathrm{H}\beta} h\nu_{\mathrm{H}\beta}}, \quad (2)$$

where n_{e} is the electron density in cm^{-3}, m_{p} is the mass of a proton in kg, L(H β) is the H β luminosity in erg s^{-1}, $\alpha^{\mathrm{eff}}_{\mathrm{H}\beta}$ is the effective recombination coefficient for H β in cm^3 s^{-1} and $h\nu_{\mathrm{H}\beta}$ is the energy of an H β photon in erg. We are assuming $T = 10\,000$ K, since this is a typical temperature for a photoionized line emitting region (Osterbrock 1989).

We apply the STARLIGHT code (Cid-Fernandes et al. 2005) to the spectrum from the optical jet emission to subtract the host galaxy contamination and AGN non-thermal continuum. Before running STARLIGHT the spectrum was corrected for Galactic extinction assuming the $E(B-v)$ values computed by Schlegel, Finkbeiner & Davis (1998). We estimate $F_{\mathrm{H}\beta} \sim 5 \times 10^{-16}$ erg s^{-1} cm^{-2}; this value should be considered as a lower limit since the width of the slit itself (1 arcsec) does not allow us to recover the entire extended emission along the jet. We consider typical densities of extended emission-line regions aligned with the radio axis that have been reported in the literature (e.g. Emonts et al. 2005; Nesvadba et al. 2006, 2008; Rosario et al. 2010b). In general, derived values for the density in extended emission-line regions – where the jet is strongly interacting with the ISM – range from 200 to 1000 cm^{-3}, which yields a mass of $10^{5.1}$ and $10^{4.4}$ M$_\odot$, respectively. This result is in agreement with previously reported masses of jet-induced outflows of ionized gas, which are of the order of 10^{4-5} M$_\odot$ (Emonts et al. 2005; Rosario et al. 2010a,b). Naturally, these values are considered as lower limits for the total outflowing gas mass, as neutral and molecular gas might be present as well.

4 DISCUSSION

We found ordered emitting gas motions along the jet of the active galaxy PKS 0521−365 with a mass of at least 10^4 M$_\odot$. Evidence of bright optical knots tightly aligned along the jet in radio galaxies has been already reported in the past; for instance, in 3C 266, 3C 324, 3C 368, 3C 371, PKS 2201+044 and PKS 2250−41 (Best et al. 1997; Scarpa et al. 1999; Villar-Martín et al. 1999; Liuzzo et al. 2011). Such alignments suggest that strong interactions are taking place between the jet and the line emitting gas, which might derive into jet-triggered star formation (Donahue et al. 2015; Tremblay et al. 2015). In this work, we report the finding of narrow-line emitting gas oriented along the jet of PKS 0521−365 and provide insights about the kinematic of these regions. We found that the gas radial velocity patterns can be well described by a sinusoidal function, giving the first spectroscopic evidence of helicoidal motions along the jet on kpc scales.

Very Long Baseline Interferometry studies have revealed that helical structures are common in extragalactic jets in pc scales (e.g. Lister et al. 2003). They are usually associated with helical magnetic fields that are linked to the rotation of the central black hole and its accretion disc together with the jet outflow (Steffen et al. 1995; Keppens et al. 2008). On the other hand, helical structures may be a consequence of jet precession caused by a supermassive binary black hole system (SBBH) or the accretion disc; the gas accretion – possibly driven by minor mergers – is likely to occur at random angles (Roos et al. 1993; Ostorero, Villata & Raiteri 2004; Lu & Zhou 2005; Aalto et al. 2016). Hence, the S-shaped jet morphologies may reflect the fact that their black hole spin axis is still precessing and has not had sufficient time to align with the accretion disc. In particular, the presence of an SBBH or recent merging activity in PKS 0521−365 remains an open question. The later models have proved to be well suited to the observations in pc scale jets, nevertheless, what remains puzzling is at what extension these models can predict a helical path. Further, theoretical and

Downloaded from https://academic.oup.com/mnrasl/article-abstract/470/1/L107/3862529
by Turun Yliopiston Kirjasto user
on 09 January 2018

observational studies are needed to reconcile these approaches with the extent of the kpc-scale jet of PKS 0521−365, which shows signs of helical structures.

PKS 0521−365 is a multifaceted object that is undergoing a high-energy episode. It represents a unique opportunity to further inspect in detail the kinetic influence and ability of radio jets to drive gas outflows and interact with the ISM of its host galaxy; in particular, to understand how radio jets can transfer energy and redistribute mass up to galactic scales, and whether they can drive star formation in the time-scales that they are acting upon the gas.

ACKNOWLEDGEMENTS

EFJ-A acknowledge support from the CONACyT (México) Master's programs and from the Collaborative Research Council 956, subproject A1, funded by the Deutsche Forschungsgemeinschaft (DFG, Germany). This work was partially supported by CONACyT research grant 151494. The observations used in this study were carried out at the European Southern Observatory (Paranal, Chile) with FORS2 on VLT (program 82.B-0720(A), PI: T. Hyvönen).

REFERENCES

Aalto S. et al., 2016, A&A, 590, 73
Appenzeller I. et al., 1998, The Messenger, 94, 1
Armus L., Soifer B. T., Murphy T. W., Jr, Neugebauer G., Evans A. S., Matthews K., 1998, ApJ, 495, 276
Best P. N., Longair M. S., Rottgering H. J. A., 1997, MNRAS, 286, 785
Cid-Fernandes R., Mateus A., Sodréé L., Stasińska G., Gomes J. M., 2005, MNRAS, 358, 363
Clark N. E., Tadhunter C. N., Morganti R., Killeen N. E. B., Fosbury R. A. E., Hook R. N., Siebert J., Shaw M. A., 1997, MNRAS, 286, 558
Clark N. E., Axon D. J., Tadhunter C. N., Robinson A., O'Brien P., 1998, ApJ, 494, 546
Collet C. et al., 2016, A&A, 586, A152
Combes F. et al., 2013, A&A, 558, A124
Croton D. J. et al., 2006, MNRAS, 365, 11
Dasyra K. M., Bostrom A. C., Combes F., Vlahakis N., 2015, ApJ, 815, 34
Donahue M. et al., 2015, ApJ, 805, 177
Emonts B. H. C., Morganti R., Tadhunter C. N., Oosterloo T. A., Holt J., van der Hulst J. M., 2005, MNRAS, 362, 931
Fabian A., 2012, ARA&A, 50, 455
Falomo R. et al., 2009, A&A, 501, 907
Giroletti M., Giovannini G., Taylor G. B., Falomo R., 2004, ApJ, 613, 752
Harrison C. M. et al., 2012, MNRAS, 426, 1073
Holt J., Tadhunter C. N., Morganti. R., 2008, MNRAS, 387, 639
Hyvönen T., Kotilainen J. K., Falomo R., Örndahl E., Pursimo T., 2007, A&A, 476, 723
Inskip K. J., Villar-Martín M., Tadhunter C. N., Morganti R., Holt J., Dicken D., 2008, MNRAS, 386, 1797
Keppens R., Meliani Z., van der Holst B., Casse F., 2008, A&A, 486, 663
King A., Pounds K., 2015, ARA&A, 53, 115
Kormendy J., Ho L. C., 2013, ARA&A, 51, 511
Krongold Y., Nicastro F., Elvis M., Brickhouse N., Binette L., Mathur S., Jiménez-Bailón Elena., 2007, ApJ, 659, 1022
Leon S., Cortes P. C., Guerard M., Villard E., Hidayat T., Ocaña F. B., Vila-Vilaro B., 2016, A&A, 586, A70
Lister M. L., Kellermann K. I., Vermeulen R. C., Cohen M. H., Zensus J. A., Ros E., 2003, ApJ, 584, 135
Liuzzo E. et al., 2011, A&A, 528, 34
Lu J.-F., Zhou B.-Y., 2005, ApJ, 635, L17
Morganti R., Fogasy J., Paragi Z., Oosterloo T., Orienti M., 2013a, Science, 341, 1082
Morganti R., Frieswijk W., Oonk R. J. B., Oosterloo T., Tadhunter C., 2013b, A&A, 552, L4
Morganti R., Oosterloo T., Oonk J. B. R., Frieswijk W., Tadhunter C., 2015, A&A, 580, A1
Nesvadba N. P. H., Lehnert M. D., Eisenhauer F., Gilbert A., Tecza M., Abuter R., 2006, ApJ, 650, 693
Nesvadba N. P. H., Lehnert M. D., De Breuck C., Gilbert A. M., van Breugel W., 2008, A&A, 491, 407
Olguín-Iglesias A. et al., 2016, MNRAS, 460, 3202
Osterbrock D. E., 1989, Astrophysics of Gaseous Nebulae and Active Galactic Nuclei. Mill Valley, California
Ostorero L., Villata M., Raiteri C. M., 2004, A&A, 419, 913
Pian E., Falomo R., Ghisellini G., Maraschi L., Sambruna R. M., Scarpa R., Treves A., 1996, ApJ, 459, 169
Press W. H., Flannery B. P., Teukolsky S. A., Vetterling W. T., 1986, Numerical Recipes. Cambridge Univ. Press, Cambridge
Querejeta M. et al., 2016, A&A, 593, A118
Roos N., Kaastra J. S., Hummel C. A., 1993, ApJ, 409, 130
Rosario D. J., Whittle M., Nelson C. H., Wilson A. S., 2010a, MNRAS, 408, 565
Rosario D. J., Whittle M., Nelson C. H., Wilson A. S., 2010b, ApJ, 711, L94
Santoro F. et al., 2015, A&A, 574
Scarpa R. R., Falomo R., Pian E., 1995, A&A, 303, 730
Scarpa R., Urry C. M., Falomo R., Pesce J. E., Webster Rachel., O'Dowd M., Treves A., 1999, ApJ, 521, 134
Schlegel D. J., Finkbeiner D. P., Davis M., 1998, ApJ, 500, 525
Solórzano-Iñarrea C., Tadhunter C. N., 2003, MNRAS, 340, 705
Steffen W., Zensus J. A., Krichbaum T. P., Witzel A., Qian S. J., 1995, A&A, 302, 335
Tremblay G. R. et al., 2015, MNRAS, 451, 3768
Urry C. M., Scarpa R., O'Dowd M., Falomo R., Pesce J. E., Treves Aldo., 2000, ApJ, 532, 816
Villar-Martín M., Tadhunter C., Morganti R., Axon D., Koekemoer A., 1999, MNRAS, 307, 24

This paper has been typeset from a TEX/LATEX file prepared by the author.

Downloaded from https://academic.oup.com/mnrasl/article-abstract/470/1/L107/3862529
by Turun Yliopiston Kirjasto user
on 09 January 2018